Journal of the European Ceramic Society 17 (1997) 55–59

PII: S0955-2219(96)00076-3
0955-2219/97/$17.00

Effect of Annealing on Phase Structure and Degradation of a Zinc Oxide Varistor with Si-additive

Hui-Qing Shao, Xiang-Hong Gao & Ze-Chun Cao*

Department of Materials Science and Engineering, Shanghai University (Jia-Ding Campus), Shanghai 201800, People's Republic of China

(Received 10 November 1994; revised version received 25 March 1996; accepted 2 April 1996)

Abstract

The effect of annealing on phase structure and degradation of the current–voltage characteristics for a ZnO varistor with Si-additive has been investigated. By means of X-ray diffraction, analytical electron microscopy and thermal analysis, it is found that a phase transition from δ-Bi_2O_3 (with dissolved Si), to $Bi_{24}Si_2O_{40}$ (bismuth silicate) took place in the ZnO varistor after annealing at 470°C. This transition is associated with a volume contraction, no notable thermal effect, a high transition rate and reversibility. It is calculated by crystallography that the volume contraction of the phase transition is 6·02%. The transition of the Bi-rich phase results in decreased levels of degradation and improved stability of the ZnO varistor. © *1996 Elsevier Science Limited.*

1 Introduction

ZnO varistors are made from ZnO doped by various metallic oxide additives, such as oxide of bismuth, antimony, cobalt and chromium. Structurally, ZnO varistors contain ZnO main phase, spinel, pyrochlore and a Bi-rich phase. Depending on the processing conditions, the Bi-rich phase may have different structures, such as α-, β- or δ-Bi_2O_3.[3,4,5] Such phases exist mainly at ZnO multigrain junctions, and sometimes spinel is embedded in ZnO grains.[10,11] All of these are actually solid solutions containing additives, such as Sb and Zn. To improve the stability of ZnO varistors, they are usually annealed or heat-preserved in the cooling procedure after sintering. When the annealing temperature approaches 450–600°C, the β- or δ-Bi_2O_3 phase transition[3,6,7] occurs and degradation of the ZnO varistor is reduced.[4,8]

*To whom correspondence should be addressed.

In practice, SiO_2 is known to be a useful additive for ZnO varistors. It affects the sintering reaction and increases the varistor voltage owing to the increased viscosity of the liquid phase during the sintering process. It exists in ZnO varistors mainly as zinc silicate (Zn_2SiO_4).[4] In this paper, by means of X-ray diffraction, thermal analysis and analytical electron microscopy, it is found that SiO_2 also affects the Bi_2O_3 phase transition after annealing at different temperatures, and the related degradation properties are studied.

2 Experimental

Reagent powders of raw materials of metallic oxides, such as Bi_2O_3, MnO, Sb_2O_3, CoO, Cr_2O_3 and SiO_2, were mixed with water and milled for 24 h. The charge was dried at 80°C, mixed with 2% adhesion agent and formed into discs using a dual-action press. The compacts were first presintered in air at 900°C and then sintered at 1260°C for 1 h. Samples were annealed in air at different temperatures, i.e. 470°C or 850°C, for 10 h and cooled in air.

The structure of samples with different heat treatments was studied by X-ray diffraction (type D/Max-rc diffractometer). In addition, on cut sections of these samples, secondary electron images and characteristic X-ray images of elements in the same area were obtained by electron probe analysis (type JCXA-733). Thermal expansion experiments and differential thermal analysis (DTA) of unannealed samples were conducted from room temperature to 900°C, using a heating rate of 5°C min^{-1}. After a pair of ohmic contacts across the samples was made using conducting resin, degradation tests were carried out using a constant dc current (10 mA). The electrode area was 25 mm^2. The level of dc degradation was

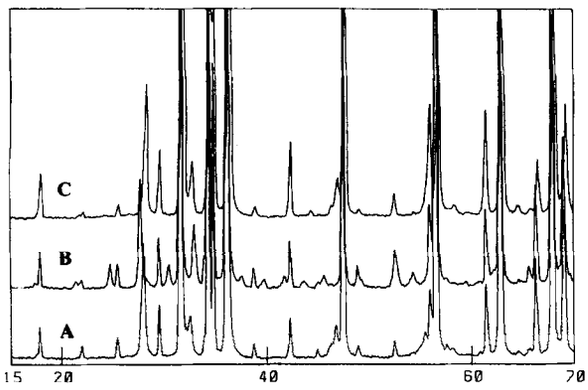

Fig. 1. XRD patterns of ZnO samples annealed at different temperatures: (A) unannealed, (B) annealed at 470°C for 10 h, (C) annealed at 850°C for 10 h.

evaluated by comparing changes between *J–E* characteristics of forwards and backwards tests for different samples.

3 Results

Figure 1 shows the X-ray diffraction (XRD) patterns of samples annealed at different temperatures. The patterns fell roughly into two categories: one included unannealed specimens and specimens annealed at 850°C; the other contained the 470°C annealed samples.

By analysing the patterns of unannealed samples in Fig. 2 and XRD data for Bi_2O_3 phase in Table 1, it appeared that the unannealed specimens contained ZnO main phase, spinel and $ZnSiO_4$, and that the Bi_2O_3 phase was δ-Bi_2O_3, not β-Bi_2O_3.[9,12] From the results presented in Fig. 3 and Table 2, it was found that annealing at 470°C caused transformation of the Bi-rich phase. Furthermore, in this case, the δ-Bi_2O_3 phase in the unannealed specimen did not transform into γ-Bi_2O_3[6,7] as is usually reported, but transformed into $Bi_{24}Si_2O_{40}$. Thus there were ZnO, spinel, $ZnSiO_4$ and $Bi_{24}Si_2O_{40}$ phases in the 470°C annealed specimens. However, after the samples were annealed at 870°C for 10 h, the structure of the Bi-rich phase was the same as that in the unannealed samples, Fig. 1.

Table 1. Powder diffraction data of three high peaks for Bi_2O_3. JCPDS file 27-52 δ-Bi_2O_3, JCPDS file 27-50 β-Bi_2O_3, and Bi_2O_3 phase in unannealed sample

δ-Bi_2O_3 (cubic)		*β-Bi_2O_3 (tetragonal)*		*Bi_2O_3 in unannealed sample*	
dA	I/I_1	dA	I/I_1	dA	I/I_1
3·19	100	3·19	100	3·191	1
2·762	38	2·737	25	2·759	2
1·9534	34	1·9626	22	1·954	3

Figure 4 compares the Bi and Si element distributions of unannealed and 470°C annealed samples obtained by electron probe analysis. To further understand the phase transformation, thermal expansion experiments and DTA were performed for the unannealed sample. As shown in Fig. 5, there was only an endothermic peak at 770°C on the DTA curve, whereas the thermal expansion curve showed a phase transition with volume contraction at 500–580°C.

The changes of *J–E* characteristics of forwards and backwards tests for degradation are compared in Fig. 6. The level of degradation of the 470°C annealed samples is obviously smaller than those of the unannealed and 870°C annealed samples, especially under reverse bias voltage. This means that the stability of the sample was improved by annealing at 470°C and reduced by annealing at 870°C.

4 Discussion

In Fig. 6 it is shown that degradation of the 470°C annealed sample, especially under reverse bias voltage, is smaller than that of the unannealed and 870°C annealed samples. Figures 2 and 3 illustrate that their diffraction patterns are different. By analysing the XRD patterns it is found that ZnO phase, spinel and $ZnSiO_4$ exist in both

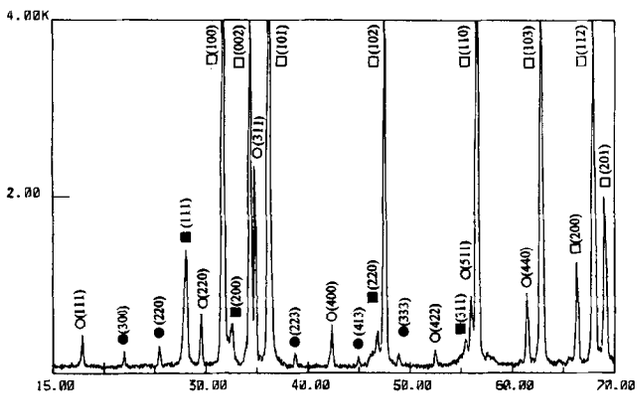

Fig. 2. XRD pattern of unannealed sample: □, ZnO; ○, spinel; ●, $ZnSiO_4$; ■, δ-Bi_2O_3.

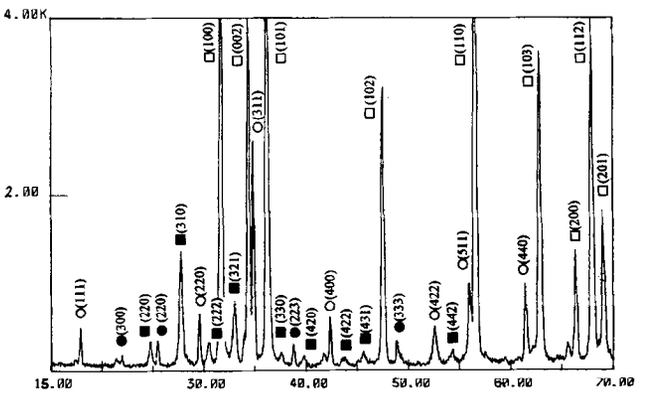

Fig. 3. XRD pattern of 470°C annealed sample: □, ZNO; ○, spinel; ●, $ZnSiO_4$; ■, $Bi_{24}Si_2O_{40}$.

Table 2. Powder diffraction data of three high peaks for Bi_2O_3, JCPDS file 29–235 γ-Bi_2O_3, JCPDS file 27–55 $Bi_{24}Si_2O_{40}$ and Bi_2O_3 phase in 470°C annealed sample

γ-Bi_2O_3 (cubic)		*$Bi_{24}Si_2O_{40}$ (cubic)*		*Bi_2O_3 in 470°C annealed sample*	
dA	I/I_1	dA	I/I_1	dA	I/I_1
3·22	100	3·20	100	3·198	1
2·73	70	2·71	90	2·707	2
1·75	45	1·73	55	1·732	3

samples, but that δ-Bi_2O_3 transforms into $Bi_{24}Si_2O_{40}$ in 470°C annealed samples. It is worth mentioning that the β- or δ-$Bi_2O_3 \rightarrow \gamma$-$Bi_2O_3$ phase transition did not occur in the above experiments, and that another Bi–rich phase (such as α–, β– and γ-Bi_2O_3) was not found, despite the power and resolution of the X-ray apparatus both being high enough. However, after samples were heated at 870°C, the diffraction pattern was the same as that of the unannealed sample.

From Fig. 4 it can be seen that the element distributions in both samples are similar. Bi and Si elements are located mainly at ZnO multigrain junctions and thus their distribution is inhomogeneous. Bi element is concentrated at ZnO multigrain junctions as Bi-rich layer and Bi-rich phase. As for Si, it exists mainly in $ZnSiO_4$ and Bi-rich phase located at multigrain junctions. This suggests that Si is also present in Bi-rich phases. In the 470°C annealed sample the Bi-rich phase is $Bi_{24}Si_2O_{40}$ (Fig. 3), and in the unannealed sample it is δ-Bi_2O_3, which dissolves Si (Fig. 2).

To get more information about this phase transition, the thermal analysis pattern was obtained from room temperature to 900°C. As shown in Fig. 5, there is a phase transition at 500–580°C that is associated with volume contraction and no apparent thermal effect. An unannealed sample that had been subjected to thermal analysis was heated up to about 680°C under the same heating rate (i.e. 5°C min^{-1}), then cooled and analysed in the X-ray diffractometer. Its XRD pattern was the same as that of 470°C annealed samples. However, after it was heated up to 850°C, its diffraction pattern was the same as that of the 870°C annealed sample. This observation is consistent with above annealing treatment; the $Bi_{24}Si_2O_{40}$ phase transformed back into δ–Bi_2O_3 phase. Therefore this phase transition is fast and reversible. Nevertheless, since the heating rate was rather high in thermal analysis, onset of the transition was delayed to a higher temperature than that for annealing treatment.

In summary, it is identified that a phase transition occurs when the material is annealed at 470°C; the exhausted phase is δ-Bi_2O_3 which dissolves Si and the product is $Bi_{24}Si_2O_{40}$. The transition is characterized by volume contraction, high transition rate but no obvious thermal effect, and its reversibility. The phase transition directly affects the varistor characteristics. In Fig. 6,

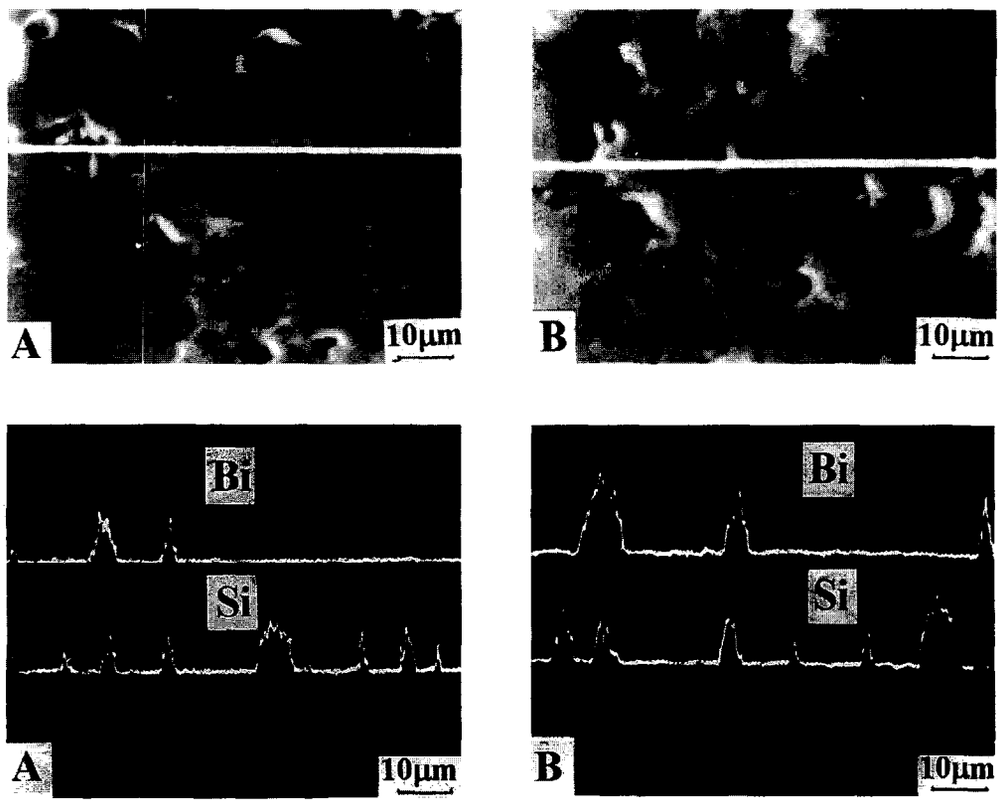

Fig. 4. Secondary-electron images and characteristic X-ray images of Bi and Si for unannealed and 470°C annealed samples.

degradation of the 470°C annealed sample was notably smaller than that of the unannealed sample, but degradation of the 870°C annealed sample increased because the reversible phase transition δ-$Bi_2O_3 \rightarrow Bi_{24}Si_2O_{40}$ took place.

Various mechanisms of degradation have been proposed to explain the difference in varistor characteristics due to the various Bi_2O_3 phases, such as 'ion migration'[13,14] and the 'stress effect'.[15] Both mechanisms are based on volume changes due to the β-Bi_2O_3 to γ-Bi_2O_3 phase transition in the multigrain junction. Phase transition would cause the 'stress effect' and then affect the varistor characteristics. Lattice constants of β-Bi_2O_3 phase (tetragonal) in the $P42_1c$ space group are a = 7.742 Å and c = 5·631 Å. Lattice constants of γ-Bi_2O_3 (cubic) in the $I23$ space group are a = 10·19 Å.[16] So the ratio of β-Bi_2O_3 to γ-Bi_2O_3 results in a volume contraction of about 3·5 vol% for Bi_2O_3[15] by crystallography. Here the α-Bi_2O_3 phase (cubic) in the $Pn2m$ space group is proposed as an oxygen-deficient CaF_2 structure. Its lattice parameter is a = 5·525 Å. The lattice constant of $Bi_{24}Si_2O_{40}$ phase (cubic) in the $I23$ space group is a = 10·10 Å.[16] The volume contraction of phase transition, as calculated by the same method, is about 6·02%.

In this work, the ratio of line contraction was obtained from the thermal expansion curve. From secondary-electron images and the characteristic X-ray image of Bi at the same region, the Bi content of the total surface was estimated. Then the volume contraction of the Bi_2O_3 phase could be calculated. The experimental value, 4·5–6·5%, is consistent with the theoretical value, 6·02%. The value is larger than the volume contraction of 3·5% due to $\beta \rightarrow \gamma$-Bi_2O_3 phase transition.[15] Because of the volume contraction of the Bi-rich phase transition at ZnO multigrain junctions, the grain boundary regions are stressed. Thus $Bi_{24}Si_2O_{40}$ may have been tensile-stressed, mainly by ZnO grains, and $Bi_{24}Si_2O_{40}$ may have stressed ZnO as a counteraction. Eventually, this process could affect the band gap or other properties, and affect the varistor characteristics. As Fig. 6 shows, the level of degradation for 470°C annealed samples is much smaller than that for unannealed samples. It has been reported that this phase dissolves Zn and Sb.[2] In this study, it is identified that it also dissolves Si. The high transition rate and absence of thermal effect imply that it is an ordering-type phase transition and $Bi_{24}Si_2O_{40}$ is actually the product to which δ-Bi_2O_3 transforms upon dissolving Si. In the ordering process, it is probable that Si occupies special lattice sites by short-range diffusion. However, the specific mechanism is not fully understood at present.

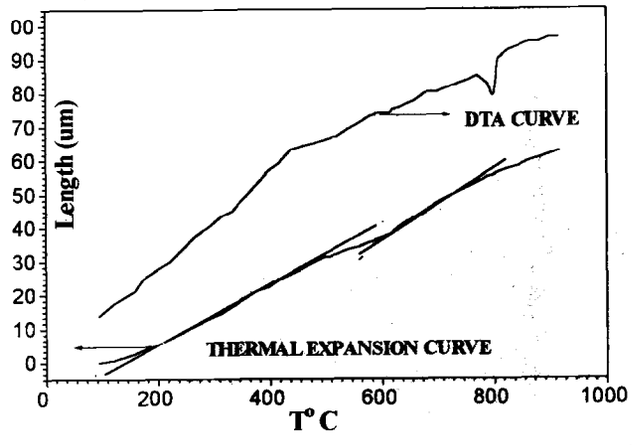

Fig. 5. Thermal expansion and DTA curves for the unannealed sample, heating rate of 5°C min^{-1}.

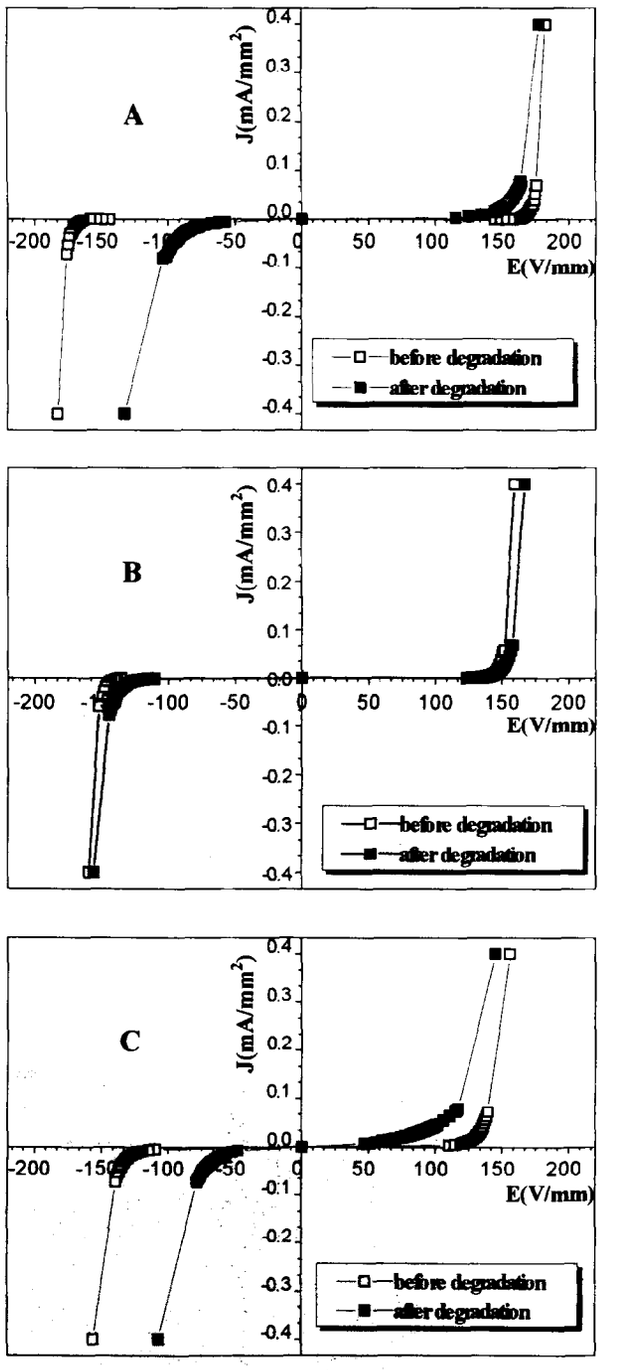

Fig. 6. J–E characteristic changes of forwards and backwards tests for degradation: (A) unannealed sample, (B) 470°C annealed sample, (C) 870°C annealed sample.

5 Conclusions

(1) With a moderate rate of cooling, δ-Bi_2O_3 which existed at high temperature could be retained at room temperature, and α- and β- Bi_2O_3 phase were not found. Si dissolved in the δ-Bi_2O_3 in unannealed sample as well as Sb and Zn.

(2) In the 470°C annealed sample, δ-Bi_2O_3 (with dissolved Si) $\rightarrow$ $Bi_{24}Si_2O_{40}$ (bismuth silicate) phase transition takes place. This transition is associated with volume contraction, no notable thermal effect, high transition rate and reversibility.

(3) The theoretical volume contraction of the δ-Bi_2O_3 $\rightarrow$ $Bi_{24}Si_2O_{40}$ phase transition is about 6·02%. It is larger than that of $\beta \rightarrow \gamma$-Bi_2O_3.

(4) The volume contraction of the Bi-rich phase transition results in improved stability and decreased level of degradation for the ZnO varistor.

Acknowledgement

Thanks are extended to The China National Nature Science Foundation and the Shanghai Natural Science Foundation for financial support. We also thank the Laboratory of Metallurgy and Materials (Shanghai University) for use of their facilities.

References

1. Inada, M., *Jpn J. Appl. Phys.*, **17**(1) (1978) 1.
2. Inada, M., *Jpn J. Appl. Phys.*, **19**(3) (1980) 409.
3. Olsson, E. & Dunlop, G. L., *J. Appl. Phys.*, **66**(9) (1989) 4317.
4. Takemura, T., Kobayashi, M., Takada, Y. & Sato, K., *J. Am. Ceram. Soc.*, **69**(5) (1987) 237.
5. Olsson, E. & Dunlop, G. L., *J. Appl. Phys.*, **60**(8) (1989) 3666.
6. Ign, A., Matusoka, M. & Masuyama, T., *Jpn J. Appl. Phys.*, **15**(6) (1976) 1161.
7. Takemura, T., Kobayashi, M., Takada, Y. & Sato, K., *Jpn J. Appl. Phys.*, **25**(2) (1986) 295.
8. Takemura, T., Kobayashi, M., Takada, Y. & Sato, K., *J. Am. Ceram. Soc.*, **70**(4) (1987) 237.
9. Wong, J., *J. Appl. Phys.*, **46**(4) (1975) 1653.
10. Asokan, T. & Freer, R., *J. Mater. Sci.*, **25** (1990) 2447.
11. Kim, J., Kimura, T. & Yamaguchi, T., *J. Mater. Sci.*, **24** (1989) 213.
12. Kim, J., Kimura, T. & Yamaguchi, T., *J. Am. Ceram. Soc.*, **72**(8) (1989) 1390.
13. Edu, K., Iga, A. & Matsuoka, M., *J. Appl. Phys.* **51**(5) (1980) 2678.
14. Hayashi, M., Haba, M., Hirano, S., Okanoto, M. & Watanabe, M., *J. Appl. Phys.*, **53**(8) (1982) 5754.
15. Takemura, T., Kobayashi, M., Takada, Y. & Sato, K., *Jpn J. Appl. Phys.*, **25**(2) (1986) 293.
16. Medernach, J. W. & Snyder, R. L., *J. Am. Ceram. Soc.*, **61**(11–12) (1978) 494–497.